Membrane Theory of a Paraboloid with an Oculus

Mitchell Gohnert[1] and Ryan Bradley[2]

Abstract: The membrane solution for the parabolic dome, or paraboloid, has been recently developed. This solution encompasses equations for both meridian and hoop stresses, for the case of gravity load and uniform shell wall thickness. Remaining to be addressed are the membrane stress equations for domes featuring an oculus, defined as a concentric circular hole at the dome's apex. The membrane equations for this case have been derived and compared to a finite-element solution, revealing a close alignment between the proposed closed-form solutions and the finite-element approximations. The only notable deviation occurs at the base, a result of boundary effects. However, these boundary effects do not impact the stresses around the opening. **DOI: 10.1061/JAEIED.AEENG-1847**.

Author keywords: Parabolic dome; Paraboloid; Oculus theory; Shell theory.

Introduction

Optimal shell structures are emerging as important structural forms and are sometimes referred to as natural structures (Gohnert 2022). Natural structures are structural systems that are found in nature; if applied to engineering designs, the results are highly efficient forms in the conveyance of stress. "Nature is a great teacher in telling us how to optimize systems" (Akbarzadeh 2023). When applied to shell structures, the stresses in natural structures are conveyed along the axis of the shell, resulting in forms that are in pure compression or tension. The most important characteristic of natural structures is that they are largely free of bending moments and shears. By eliminating the bending moments and shears, the magnitude of stress is greatly reduced, the stress capacity against failure is dramatically increased, and lesser materials are required in the construction of the dome. These favorable characteristics are the reasons why domes are some of the only structures that have survived from antiquity.

Forms, patterned after natural shapes, are not new but were originally envisioned by the famed scientist Robert Hooke back in 1775. The idea was mooted by the study of a draping chain (Block et al. 2006), which was revolved 360° to form a dome. A draping chain creates a unique natural form that is free of bending and shears; the stresses are in pure tension, and if flipped upright, the flow of force is reversed and in pure compression. Hooke's postulate was applied to the dome of St. Paul's Cathedral in the same year of discovery and is considered a ground-breaking achievement of engineering innovation. Originally, Hooke thought that the shape followed a cubic parabola, which was a good approximation, but not exact (Heyman 1998). In later years, the shape of a draping chain was proved to be a hyperbolic cosine function, independently determined by Leibniz, Huygens, and Bernoulli (Saouma 2022). Despite the error in Hooke's original hypothesis, the two forms are similar in geometry and the way stresses flow in the shell (Kaplan 2008).

The membrane resultant stress equations for both the catenary and parabolic domes have recently been developed (Gohnert and Bradley 2023; Gohnert and Bradley 2022). The equations for the catenary dome, however, have been further developed by including solutions for an oculus, and a variation in shell thickness (Gohnert and Bradley 2021). At present, only the membrane theory for the paraboloid has been developed, for a dome without openings. What remains is the development of an oculus theory for the paraboloid, which is the focus of this article. As with all oculus theories, the hole is circular, concentric, and located at the apex of the dome (Billington 1982) while the dome remains stable, irrespective of the size of the opening. An oculus has several functions: First, an oculus provides natural light into the dome. The pantheon in Rome and lanterns built on top of cathedrals are prime examples, but in more modern times a translucent skylight would be fitted into the opening. Second, an oculus lightens the dome and provides a more economical solution where only a portion of the dome requires a covering (e.g., sports areas).

As with all closed-form solutions, these equations provide verification of an analysis and measure the quality of the numerical solution (i.e., finite elements). Ironically, a finite-element (FE) analysis is also used to verify closed-form solutions, albeit it is an approximation. It is common practice to use finite elements, or other methods, such as the boundary-element methods (Gaul et al. 2003), to evaluate the quality of the proposed solutions. Therefore, the derived equations are compared with a finite-element analysis, which is given at the end of the derivation.

Geometrical Relationships

y-Dimension of the Dome

Referring to Fig. 1, the y-dimension of the parabolic curve is given by (Stroud 1995)

$$y_1 = x^2/4P \tag{1}$$

[1]Professor, School of Civil and Environmental Engineering, Univ. of the Witwatersrand, PO Wits, Johannesburg 2050, South Africa (corresponding author). ORCID: https://orcid.org/0000-0002-8258-7284. Email: mitchell.gohnert@wits.ac.za

[2]Senior Lecturer, School of Civil and Environmental Engineering, Univ. of the Witwatersrand, PO Wits, Johannesburg 2050, South Africa. ORCID: https://orcid.org/0000-0003-4988-7143. Email: ryan.bradley@wits.ac.za

Note. This manuscript was submitted on March 2, 2024; approved on October 11, 2024; published online on December 10, 2024. Discussion period open until May 10, 2025; separate discussions must be submitted for individual papers. This paper is part of the ***Journal of Architectural Engineering***, © ASCE, ISSN 1076-0431.

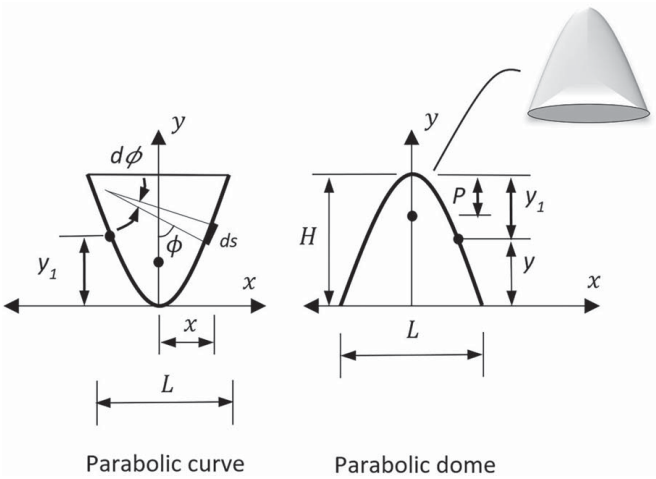

Fig. 1. Geometry of the parabolic curve and dome.

where P = focal point, in terms of the span L and the height H.

$$P = L^2/16H \tag{2}$$

The height y for the dome is given by

$$y = H - y_1 \tag{3}$$

Substituting Eq. (1) into (3), the y-dimension of the dome is determined as follows:

$$y = H - x^2/4P \tag{4}$$

Relationship between the Horizontal Radius x and Meridian Angle

Taking the derivative of Eq. (1)

$$dy_1/dx = x/2P \tag{5}$$

And the second derivative, which will be used later in the derivation

$$d^2y_1/dx^2 = 1/2P \tag{6}$$

The change in y with respect to x is also equal to the tangent of the meridian angle φ. Therefore

$$\tan\phi = x/2P \tag{7}$$

Rearranged, we get

$$\phi = \tan^{-1}(x/2P) \tag{8}$$

The angle at the oculus

$$\phi_o = \tan^{-1}(x_o/2P) \tag{9}$$

where

$$\phi \geq \phi_o$$

Curvature k and Radius r of the Parabolic Curve

The curvature of the parabolic curve may be solved from the following generic curvature equation:

$$k = \frac{\left(\frac{d^2y}{dx^2}\right)}{\left[1 + \left(\frac{dy}{dx}\right)^2\right]^{3/2}}$$

Substituting Eqs. (5) and (6) into the aforementioned equation, we get

$$k = \frac{\left(\frac{1}{2P}\right)}{\left[1 + \left(\frac{x}{2P}\right)^2\right]^{3/2}} \tag{10}$$

Simplifying Eq. (10), the radius is the reciprocal of the curvature, as follows:

$$r = \frac{1}{k} = 2P\sqrt{\left(1 + \frac{x^2}{4P^2}\right)^3} \tag{11}$$

Weight of the Dome Cap Removed

The dome cap is the portion of the dome above the oculus opening, as illustrated in Fig. 2. To solve the stresses in the dome, the weight of the dome cap must be removed from the stress equations. Thus, determining the weight of the dome is necessary to solve the stresses in the dome with an oculus. Furthermore, an upside-down paraboloid is used to ease the complexity of the calculations. The equation for the dome cap may be determined by integrating the differential rings as follows (Billington 1982):

$$R_o = \int_0^{x_o} q\ 2\pi x\ ds \tag{12}$$

where q = self-weight of the dome per surface area; ds = width of the differential ring; and x_o = radius of the opening or oculus.

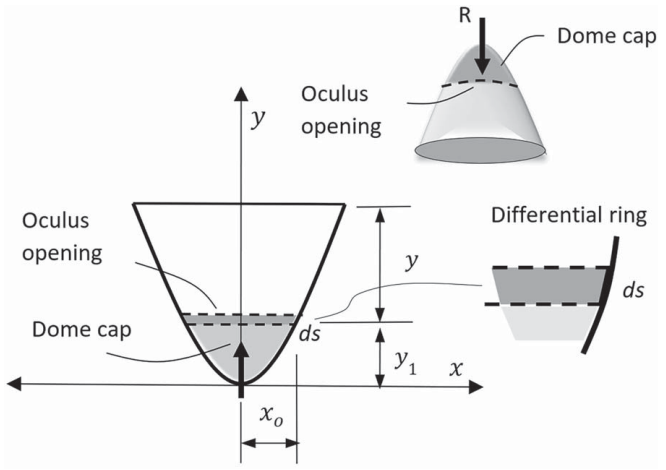

Fig. 2. Oculus and dome cap.

Referring to Fig. 2 and using the Pythagorean theorem, the width of the ring ds is defined in terms of the radius x as follows:

$$ds = \sqrt{1 + (dy_1/dx)^2}\, dx \tag{13}$$

Substituting Eq. (5) into (13), we get

$$ds = \sqrt{1 + (1/4P^2)x^2}dx \tag{14}$$

The calculations are eased by the substitution of α as follows:

$$\alpha = 1/4P^2 \tag{15}$$

Replacing the ds and removing the constants from the integrand, we get

$$R_o = 2\pi q \int_0^{x_o} x\sqrt{1 + \alpha x^2}\, dx \tag{16}$$

Solve the integral by the method of integration substitution. Let

$$u = 1 + \alpha x^2 \tag{17}$$

Therefore

$$du = 2\alpha x\, dx$$

Or

$$xdx = du/2\alpha \tag{18}$$

Solving for the integration interval, using Eq. (17), we get

$$\text{At } x = 0, \quad u = 1 \tag{19}$$

$$\text{At } x = x_o, \quad u = 1 + \alpha x_o^2 \tag{20}$$

Substitute Eqs. (17) and (18), and the integration interval Eqs. (19) and (20) into (16)

$$R_o = \frac{\pi q}{\alpha} \int_1^{1+\alpha x_o^2} \sqrt{u}\, du \tag{21}$$

Integrate Eq. (21)

$$R_o = \frac{\pi q}{\alpha}\left[\frac{2}{3}u^{3/2}\right]_1^{1+\alpha x_o^2}$$

Evaluate and substitute u back into the integral. The equation for the dome cap is therefore solved

$$R_o = \frac{2\pi q}{3\alpha}\left[\sqrt{(1 + \alpha x_o^2)^3} - 1\right] \tag{22}$$

Using this same equation, the weight of the dome cap is expressed as follows:

$$R = \frac{2\pi q}{3\alpha}\left[\sqrt{(1 + \alpha x^2)^3} - 1\right] \tag{23}$$

where $x_o \le x \le L/2$.

Meridian Stress

The meridian stress is determined by dividing the weight of the dome by the circumference length. Furthermore, the equation is divided by $\sin\phi$ to align the gravity load with the direction of the membrane stress

$$N'_\phi = -\frac{R}{2\pi x \sin\phi} \tag{24}$$

The aforementioned equation, however, is the equation for a dome without an oculus and was previously applied to circular domes (Billington 1982). To determine the membrane stresses in the dome, which includes oculus theory, Eq. (24) is altered by removing the weight of the dome cap above the oculus (Fig. 3)

$$N'_\phi = -\frac{(R - R_o)}{2\pi x \sin\phi} \tag{25}$$

Solving for $R - R_o$, we get

$$R - R_o = \frac{2\pi q}{3\alpha}\left[\sqrt{(1 + \alpha x^2)^3} - 1\right] - \frac{2\pi q}{3\alpha}\left[\sqrt{(1 + \alpha x_o^2)^3} - 1\right] \tag{26}$$

Replace α in the brackets, in Eq. (15), to get

$$R - R_o = \frac{2\pi q}{3\alpha}\left[\sqrt{\left(1 + \frac{x^2}{4P^2}\right)^3} - 1\right] - \frac{2\pi q}{3\alpha}\left[\sqrt{\left(1 + \frac{x_o^2}{4P^2}\right)^3} - 1\right] \tag{27}$$

Since $\tan\phi = x/2P$ [Eq. (7)]

$$R - R_o = \frac{2\pi q}{3\alpha}\left[\sqrt{(1 + \tan^2\phi)^3} - 1\right] - \frac{2\pi q}{3\alpha}\left[\sqrt{(1 + \tan^2\phi_o)^3} - 1\right] \tag{28}$$

$$R - R_o = \frac{2\pi q}{3\alpha}\left[\sqrt{(\sec^2\phi)^3} - 1\right] - \frac{2\pi q}{3\alpha}\left[\sqrt{(\sec^2\phi_o)^3} - 1\right] \tag{29}$$

$$R - R_o = \frac{2\pi q}{3\alpha}(\sec^3\phi - \sec^3\phi_o) \tag{30}$$

Substituting Eq. (30) into (25), we get

$$N'_\phi = -\frac{q}{3\alpha x \sin\phi}(\sec^3\phi - \sec^3\phi_o) \tag{31}$$

Note that $\alpha = 1/4P^2$ [Eq. (15)] and Eq. (7) can be rearranged as $x = 2P\tan\phi$. Making these substitutions

$$N'_\phi = -\frac{2qP}{3\tan\phi\sin\phi}(\sec^3\phi - \sec^3\phi_o) \tag{32}$$

where $\phi \ge \phi_o$.

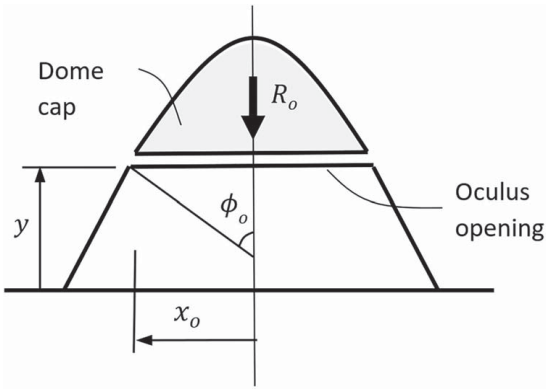

Fig. 3. Dome cap and oculus.

Hoop Stress

The hoop equation is determined by summing the forces in the radial direction (normal to the surface of the dome). The forces are solved by multiplying the membrane stresses (Fig. 4) by the lengths of the differential element (Fig. 5). The components of the force, in the radial direction, are determined by using sin functions (Fig. 6).

Summing the forces

$$N'_\phi x d\theta \sin\frac{d\phi}{2} + \left(N'_\phi + \frac{\partial N'_\phi}{\partial \phi}d\phi\right)\left(x + \frac{\partial x}{\partial \phi}d\phi\right)d\theta \ \sin\frac{d\phi}{2} + N'_\phi r d\phi \sin\frac{d\theta_1}{2} + N'_\phi r d\phi \sin\frac{d\theta_1}{2} + P_z \ r d\phi \ x d\theta = 0 \tag{33}$$

where P_z = pressure normal to the surface of the dome. Because differential elements are infinitesimal, the sin of the angle is approximately equal to the angle as follows:

$$\sin\frac{d\phi}{2} = \frac{d\phi}{2}$$

$$\sin\frac{d\theta_1}{2} = \frac{d\theta_1}{2}$$

Making this substitution and expanding Eq. (33), we get

$$N'_\phi x d\theta \ \frac{d\phi}{2} + N'_\phi x d\theta \ \frac{d\phi}{2} + N'_\phi \frac{\partial x}{\partial \phi}d\phi \ d\theta \ \frac{d\phi}{2} + \frac{\partial N'_\phi}{\partial \phi}d\phi \ x \ d\theta \frac{d\phi}{2} + \frac{\partial N'_\phi}{\partial \phi}d\phi \ \frac{\partial x}{\partial \phi} \ d\phi \ d\theta \frac{d\phi}{2} + N'_\theta r \ d\phi \ \frac{d\theta_1}{2} + N'_\theta r \ d\phi \ \frac{d\theta_1}{2} + P_z r x \ d\phi \ d\theta = 0 \tag{34}$$

Simply by combining like terms and eliminating the higher-order terms (i.e., terms that are much smaller in magnitude), Eq. (34) simplifies to

$$N'_\phi x d\theta \ d\phi + N'_\theta r \ d\phi \ d\theta_1 + P_z r x \ d\phi \ d\theta = 0 \tag{35}$$

The relationship between angles θ_1 and ϕ is determined by equating the top length of the differential element. Referring to Fig. 5

$$r_2 \ d\theta_1 = x \ d\theta$$

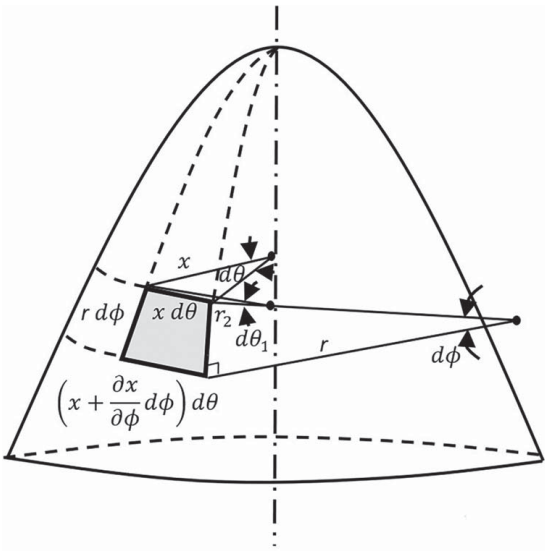

Fig. 5. Lengths of the differential element.

Rearranged, we get

$$d\theta_1 = \frac{x \ d\theta}{r_2}$$

Making this substitution and dividing by $d\theta \ d\phi$, we get

$$N'_\phi x + \frac{N'_\theta r x}{r_2} + P_z r x = 0 \tag{36}$$

Rearrange to solve for the hoop stress, which is similar to the hoop stress equation developed for the circular dome (Billington 1982)

$$N'_\theta = \frac{-r_2}{r}(N'_\phi + P_z r) \tag{37}$$

The radial pressure (P_z) is related to the gravity load q by the cosine of the meridian angle. Furthermore, the radius r_2 is related to the horizontal radius x by the following expression:

$$P_z = q \cos\phi \tag{38}$$

$$x = r_2 \sin\phi$$

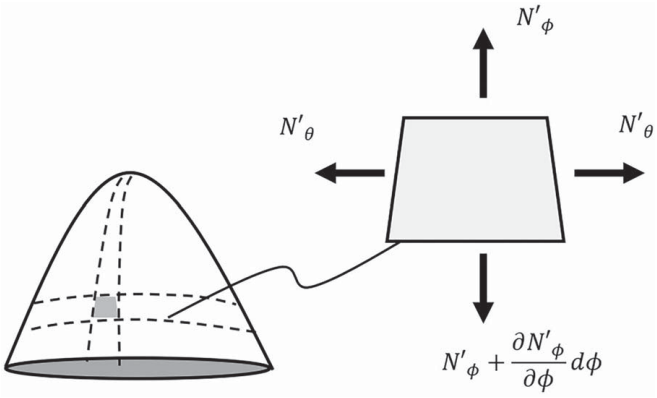

Fig. 4. Membrane stresses along the edges of the differential element.

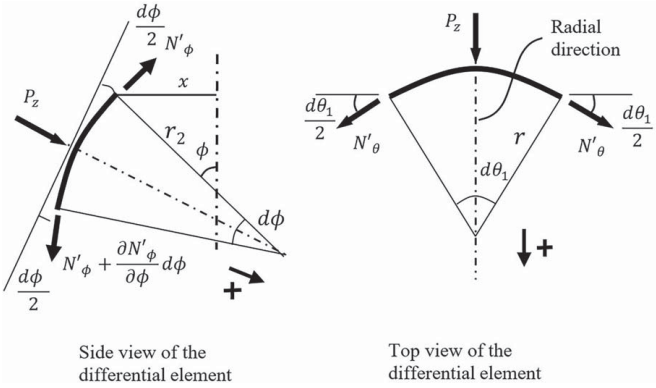

Fig. 6. Orientation of the stresses along the edges of the differential elements.

Or

$$r_2 = x/\sin\phi \tag{39}$$

Substituting Eqs. (38) and (39), and rearranging, we get

$$N'_\theta = -x\left(\frac{N'_\phi}{r}\csc\phi + q\cot\phi\right) \tag{40}$$

Substitute Eq. (32) into (40) to get

$$N'_\theta = -x\left[\frac{-2qP(\sec^3\phi - \sec^3\phi_o)}{r\ 3\tan\phi\sin\phi}\csc\phi + q\cot\phi\right] \tag{41}$$

$$N'_\theta = \frac{qx}{\sin\phi}\left[\frac{2P(\sec^3\phi - \sec^3\phi_o)}{3\ r\tan\phi}\csc\phi - \cos\phi\right] \tag{42}$$

$$N'_\theta = qx\cot\phi\left[\frac{2P}{3\ r\ \sin^2\phi}(\sec^3\phi - \sec^3\phi_o) - 1\right] \tag{43}$$

Replace the coordinate x using $x = 2P\tan\phi$ [Eq. (7)]

$$N'_\theta = 2qP\left[\frac{2P}{3\ r\sin^2\phi}(\sec^3\phi - \sec^3\phi_o) - 1\right] \tag{44}$$

where $\phi \geq \phi_o$.

Comparison of Oculus Theory and Finite-Element Solutions

To investigate the impact of edge effects not captured by the proposed membrane solution, an FE analysis was conducted using the Abaqus/CAE (version 2020) software package (Dassault Systèmes 2020). This study assessed the stress distributions in both hoop and meridian directions, derived from a full-shell analysis that incorporates both in-plane (membrane) and bending behavior. The results were then compared to the membrane stresses derived from the proposed equations. FE simulations were executed on a quarter-section of a full dome model to exploit geometric and load symmetries. Boundary conditions were applied along the model's three restrained edges: the base was fixed against all

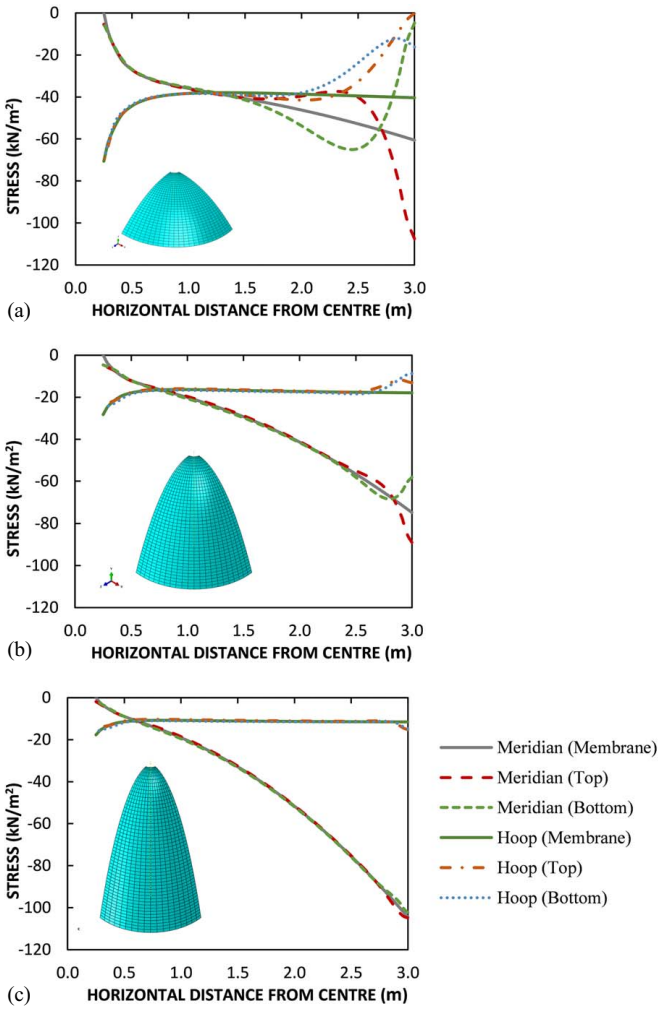

Fig. 7. FE hoop and meridian stresses plotted alongside the proposed membrane stresses [$t = 100$ mm and $(x_o) = 0.25$ m]. (Top—inside surface; bottom—outside surface): (a) $H/L = 0.25$; (b) $H/L = 0.625$; and (c) $H/L = 1.00$.

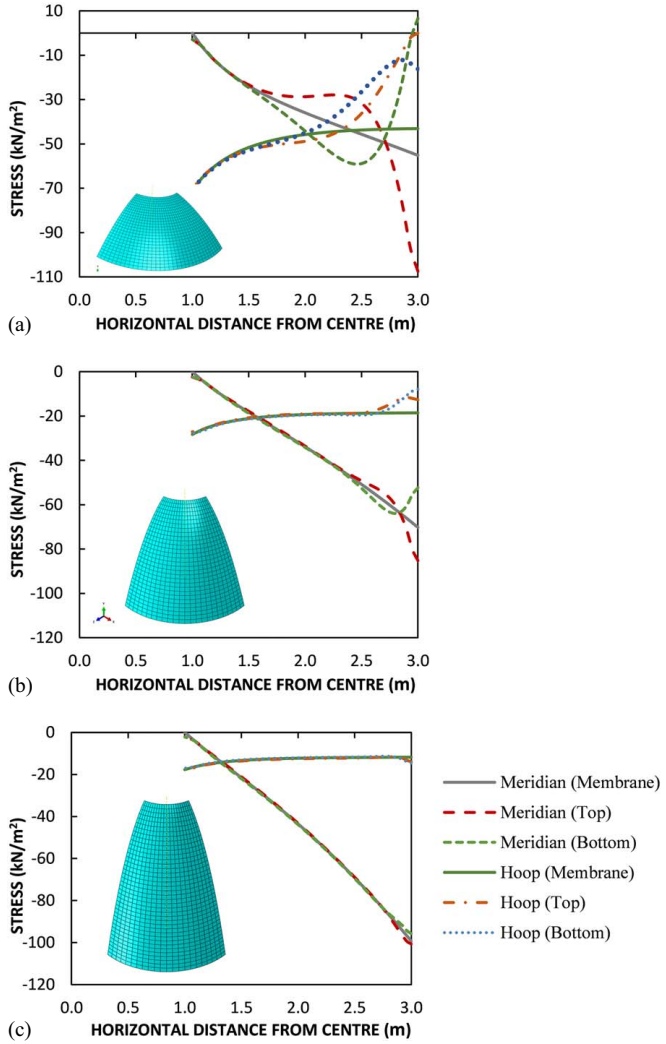

Fig. 8. FE hoop and meridian stresses plotted alongside the proposed membrane stresses [$t = 100$ mm and $(x_o) = 1.0$ m]: (a) $H/L = 0.25$; (b) $H/L = 0.625$; and (c) $H/L = 1.00$.

rotations and displacements (encastre), and the two continuous edges were constrained with appropriate displacement and rotational restrictions. The analyses utilized conventional S4 shell elements with a suitably refined and structured mesh to ensure the required accuracy.

1. The scope of comparisons in this study is limited, acknowledging the need for brevity as well as results published in prior investigations (Gohnert and Bradley 2023, Gohnert 2022, Bradley and Gohnert 2022, Gohnert and Bradley 2021) on the influence of various model parameters on the stress distributions in paraboloids and catenary domes, including Young's modulus (E), Poisson's ratio (v), height-to-span ratio (H/L), and shell thickness (t). The main observations from the FE analyses presented in those studies, relevant to small concrete paraboloid or catenary domes and similarly applicable to those incorporating an oculus, are reported herein: Poisson's ratio (v) exhibits a notable impact on edge effects, specifically the extent and magnitude of bending and boundary forces. However, within the anticipated range of Poisson's ratio for concrete, typically between 0.1 and 0.2 (Beushausen et al. 2021), this influence is comparatively minor.
2. By contrast, the value of Young's modulus has no impact on either hoop or meridian stress distributions.
3. The H/L ratio significantly affects the extent and magnitude of edge effects in paraboloid domes. Specifically, shallow domes exhibit considerably more bending than their steeper counterparts.
4. An increase in shell thickness has a noticeable influence on both the extent and intensity of boundary effects, with thicker shells exhibiting more pronounced boundary action. This trend was noted across a range of catenary dome configurations, whether they included a concentric opening or not, as documented in two previous studies (Gohnert 2022; Bradley and Gohnert 2022).

The influence of the H/L ratio, t, and the radius of the dome opening (x_o) on stress distributions was considered in the subsequent analyses. The thickness varied between 100 and 200 mm, while several radii of the oculus and H/L ratios were considered. The material parameters remained constant throughout the study. An H/L ratio of 0.75, corresponding to a height and span of 4.5 and 6 m, respectively, was selected for the additional investigations on shell thickness and oculus radius. Portions of the shell were cut away from the paraboloid to achieve the various oculus openings in the FE models. Concrete was specified as the material for all models, with an E of 30 GPa and a v of 0.15.

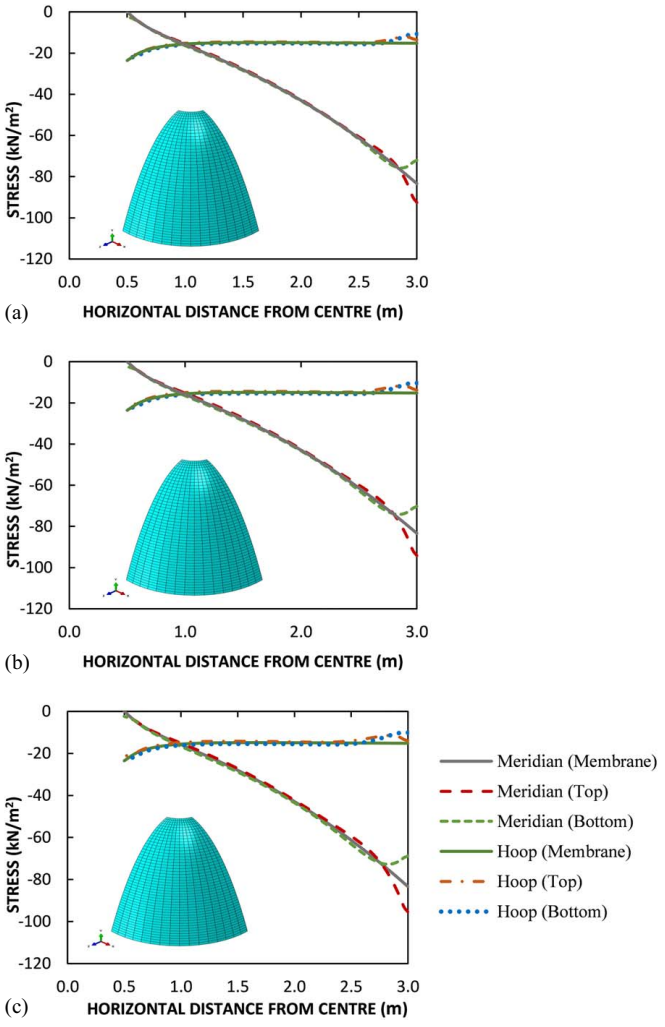

Fig. 9. FE hoop and meridian stresses plotted alongside the proposed membrane stresses [$(H/L) = 0.75$ and $(x_o) = 0.5$ m]: (a) $t = 100$ mm; (b) $t = 150$ mm; and (c) $t = 200$ mm.

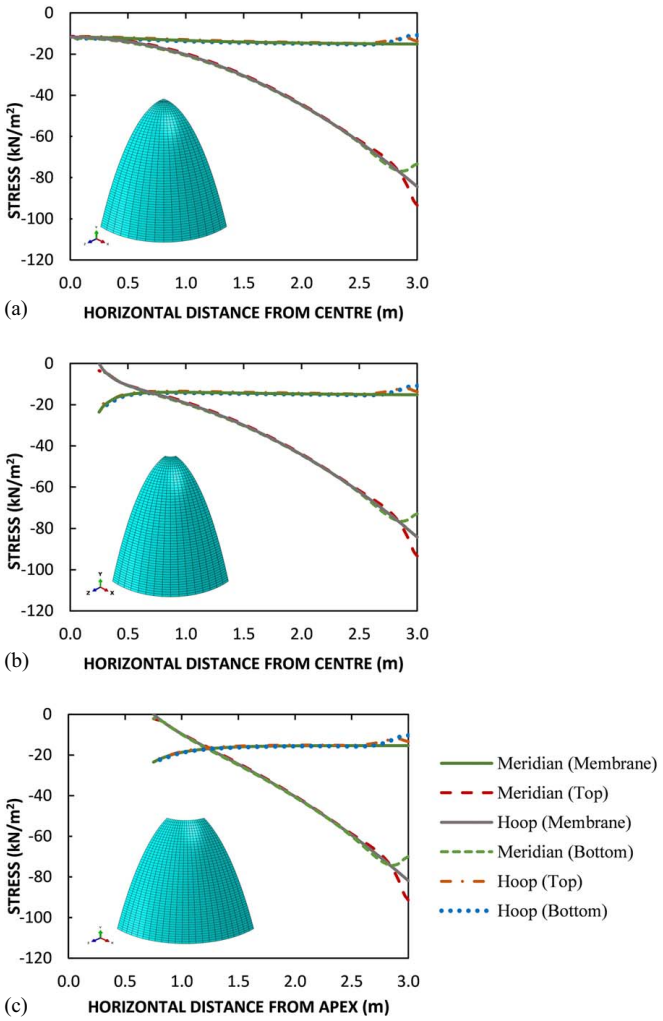

Fig. 10. FE hoop and meridian stresses plotted alongside the proposed membrane stresses. Oculus diameter up to 25% of the dome diameter [$(H/L) = 0.75$ and $t = 100$ mm]: (a) no oculus, $x_o = 0$; (b) $x_o = 0.25$ m; and (c) $x_o = 0.75$ m.

It has been previously established that in very shallow parabolic domes that are restrained at their base—whether they are pinned, supported by a ring beam, or fixed—bending and boundary forces predominate the stress distributions (Gohnert and Bradley 2023). This is clearly apparent in Figs. 7(a) and 8(a), which show the membrane and FE stresses for a shallow paraboloid with oculus radii of 0.25 and 1.0 m, respectively. The disparity between the meridian stresses is significant, which is predominantly due to bending action. By contrast, the difference in hoop stresses is primarily due to in-plane boundary force. Both effects quickly diminish as the dome becomes steeper, as shown in Figs. 7(b) and 8(b). This is especially apparent as the H/L ratio exceeds 1.0 [Figs. 7(c) and 8(c)]. In fact, the proposed membrane theory provides a reasonable approximation of internal stresses in steeper paraboloids under gravity load.

Figs. 9(a–c) show the distributions of hoop and meridian stresses within a paraboloid featuring an oculus with a 0.5 m radius, across different shell thicknesses. As expected, variations in the shell thickness did not affect the membrane solutions. Conversely, it is evident that an increase in thickness had a visible influence on both the extent and intensity of boundary effects determined with FE analyses. However, the significance of this impact remains minor for the small dome in question. Similar observations were noted for other H/L ratios, but these are not included here for reasons of brevity.

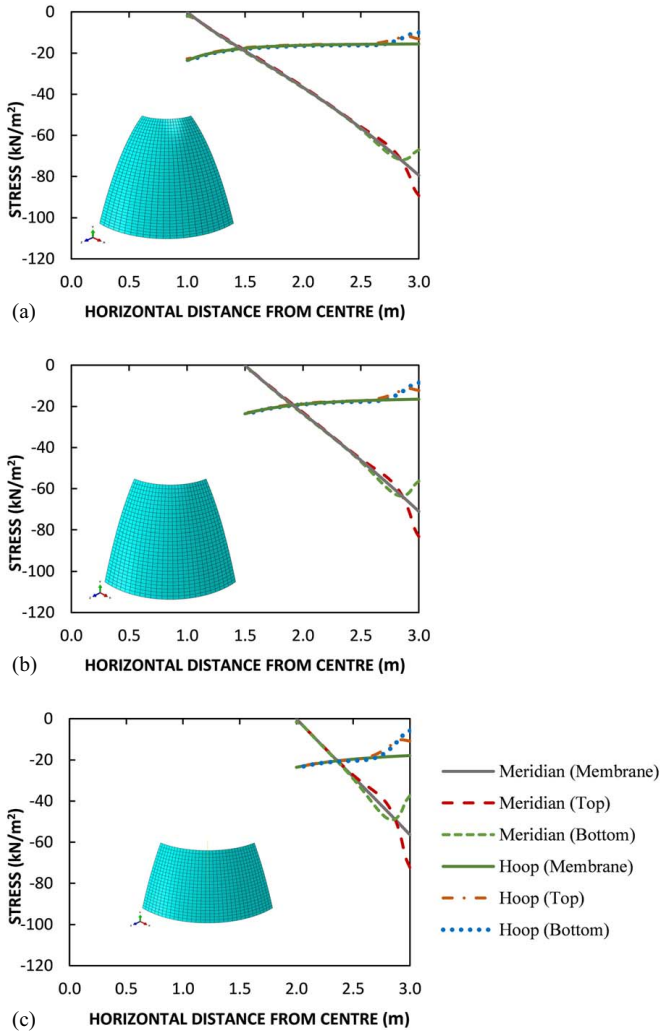

Fig. 11. FE hoop and meridian stresses plotted alongside the proposed-membrane stresses. Oculus diameter between 33% and 67% of the dome diameter [$(H/L) = 0.75$ and $t = 100$ mm]: (a) $x_o = 1.0$ m; (b) $x_o = 1.5$ m; and (c) $x_o = 2.0$ m.

Figs. 9(a) and 10(a–c) depict the hoop and meridian stresses alongside the membrane solutions for various oculus radii within a steep paraboloid of 100 mm thickness. The opening radius was varied from 0 to 0.75 m (or up to 25% of the dome's radius), in increments of 0.25 m. The proportions of these oculi, in relation to the dome itself, are consistent with those observed in ancient unreinforced domes, such as the dome of the Pantheon (Encyclopedia Britannica 2004), and modern examples, including the earth masonry domes of the Mapungubwe Interpretation Centre (Fagan 2010). Several interesting observations can be made when comparing Figs. 9(a) and 10(a–c), as follows: (1) boundary effects are not apparent around or near the oculus; (2) boundary effects are limited to a zone near the base of the steep dome; and (3) the magnitude of the boundary effects is similar across the domes. As such, the advantage of utilizing the paraboloid shape is equally evident for paraboloids featuring an oculus.

The results presented in Fig. 11, however, introduce a caveat for domes featuring overly large openings. Specifically, even steep paraboloids with large concentric openings exhibit increased boundary effects toward their base, as illustrated in Fig. 11(c). This outcome was anticipated, as the form has deviated from what might traditionally be considered a dome; a curved, inclined wall may offer a more accurate description. Nonetheless, the paraboloids examined in Figs. 11(b and c) remain in pure compression, regardless of the large oculus dimensions.

Conclusions

The stress equations for the parabolic dome were derived with the objective of developing shell forms that are optimal, in the conveyance of stress. These types of shells are sometimes called natural structures, because the geometric profile follows the natural flow of stress. The adaptation of oculus theory expands the versatility of the parabolic dome and enables an understanding of the limits of application and the influence of boundary conditions.

The membrane theory for the paraboloid has been previously developed for a uniformly thick shell, subjected to gravity loads (Gohnert and Bradley 2023). The proposed solution, which includes oculus theory, is also a membrane solution and assumes that the base is unrestrained to sliding. In reality, the boundary will be pinned or fixed to an edge beam or foundation. The finite-element study therefore considers the accuracy of the equations and the influence of boundary effects. As a result of the study, the only difference observed was some deviation at the support, owing to base restraint of the finite-element model, but the discrepancies between the two solutions were found to be minor in most analyses. The finite-element study did however show that Poisson's ratio, the variation in height to span, and size of the oculus opening do influence the extent and magnitude of the boundary effects:

1. As with all dome shapes, the edge effects in shallow domes are more prominent. The extreme case is a flat dome, or slab, where most of the load is carried by bending and shears. The parabolic dome is no different (with or without an oculus), where stresses transition from arching action to bending and shears as the shape flattens.
2. A study of very large openings indicates a divergence in stresses near the boundary. However, the geometry investigated is extreme, and it is questionable if the dome is still a dome, or a curved wall. Nevertheless, the study is useful to determine the limits of the proposed theory.

In comparison with other domes, the paraboloid is similar to the catenary dome. The stresses in the parabolic dome are compression

and boundary effects are minimal. Within the range of finite-element studies, the diameter of the oculus had a minor influence on boundary effects. However, significant divergence is apparent in shallow domes, with or without an oculus, where bending and boundary forces dominate the stress distributions. In such cases, the boundary effect cannot be disregarded and their inclusion in the closed-form solution should be contemplated in future research. In summary, the membrane equations of the parabolic dome with an oculus provide an accurate solution in most cases.

The study and proposed theory are based on an elastic/linear analysis of a parabolic dome. The next stage of development is a nonlinear solution, which may include theories proposed by Heyman (1995).

Data Availability Statement

Some or all data, models, or codes that support the findings of this study are available from the corresponding author upon reasonable request.

References

Akbarzadeh, M. 2023. "Natural structures can give us rise to stronger, lighter systems." *Pen Today*, July 18, 2023.

Beushausen, H., P. Arito, G. van Zijl, and M. G. Alexander. 2021. "*Deformation and volume change of hardened concrete*." In *Fulton's concrete technology*. 10th ed., edited by M. G. Alexander, 211–288. Johannesburg, South Africa: The Concrete Institute.

Billington, D. P. 1982. *Thin shell concrete structures*. New York: McGraw-Hill.

Block, P., M. Dejong, and J. Ochendorf. 2006. "As hangs the flexible line: Equilibrium of masonry structures." *Nexus Network J.* 8 (2): 13–24. https://doi.org/10.107/s00004-006-0015-9.

Bradley, R. A., and M. Gohnert. 2022. "Parametric study of a catenary dome under gravitational load." In *Proc., 8th Int. Conf. on Structural Engineering, Mechanics, and Computation*. Lodon, UK: CRC Press.

Dassault Systèmes. 2020. *Abaqus/CAE 2020 [software]*. Johnston, RI: Dassault Systèmes.

Encyclopedia Britannica. 2024. "Pantheon." In *Encyclopedia Britannica*. Accessed February 25, 2024. https://www.britannica.com/topic/Pantheon-building-Rome-Italy.

Fagan, G. 2010. "Mapungubwe Interpretation Centre by Peter Rich Architects, Mapungubwe National Park, South Africa." *The Architectural Review*. Accessed February 25, 2024. https://www.architectural-review.com/today/mapungubwe-interpretation-centre-by-peter-rich-architects-mapungubwe-national-park-south-africa.

Gaul, L., M. Kogl, and M. Wagner. 2003. *Boundary element method for engineers and scientist: An introductory course with advanced topics*. Berlin, Germany: Verlag Springer.

Gohnert, M. 2022. "The natural flow of stress in shell structures." In *Proc., 7th Int. Conf. on Civil, Structural and Transportation Engineering*. Orleans, ON: International ASET Inc.

Gohnert, M., and R. Bradley. 2021. "Membrane solution for a catenary dome." *J. Int. Assoc. Shell Spatial Struct.* 62: 37–49. https://doi.org/10.20898/j.iass.2020.003.

Gohnert, M., and R. Bradley. 2022. "Membrane stress equations for a catenary dome with a variation in wall thickness." *Eng. Struct.* 253: 113793. https://doi.org/10.1016/j.engstruct.2021.113793.

Gohnert, M., and R. Bradley. 2023. "Membrane solution for a paraboloid under self-weight." *J. Int. Assoc. Shell Spatial Struct.* 64 (3): 240–248. https://doi.org/10.20898/j.iass.2023.017.

Heyman, J. 1995. *The stone skeleton—Structural engineering of masonry architecture*. Cambridge, UK: Cambridge University Press.

Heyman, J. 1998. "Hooke's cubico-parabolical conoid." *Notes Rec. R. Soc. London* 52 (1): 39–50. https://doi.org/10.1098/rsnr.1998.0033.

Kaplan, G. 2008. *The catenary art, architecture, history, and mathematics*, 47–54. Towson, Maryland: Dept. of Mathematics, Towson Univ.

Saouma, V. E. 2022. *History of structural analysis: Personal perspective*. Cham, Switzerland: Springer Nature.

Stroud, K. A. 1995. *Engineering mathematics*. 4th ed. London: Macmillan.